Available online at www.sciencedirect.com
ScienceDirect
Ceramics International 38 (2012) 433–441
CERAMICS INTERNATIONAL
www.elsevier.com/locate/ceramint

Creep behaviour of alumina/YAG composites prepared by different sintering routes

P. Palmero [a,*], G. Fantozzi [b], F. Lomello [a,1], G. Bonnefont [b], L. Montanaro [a]

[a] Department of Material Science and Chemical Engineering, Politecnico di Torino, INSTM, R.U. PoliTO, LINCE Lab., C.so Duca degli Abruzzi 24, 10129 Torino, Italy

[b] Université de Lyon, INSA de Lyon, MATEIS UMR CNRS 5510, Bât. Blaise Pascal, 7 Av. Jean Capelle, 69621 Villeurbanne, France

Received 24 May 2011; received in revised form 12 July 2011; accepted 12 July 2011
Available online 29th July 2011

Abstract

Al_2O_3–5 vol.% $Y_3Al_5O_{12}$ (YAG) composite powders have been prepared by surface doping of α-alumina powders by an yttrium chloride aqueous solution. Two commercial, one submicron-sized, the other ultra-fine, alumina powders were compared as matrix materials. YAG phase was yielded by an in situ reaction promoted by the subsequent thermal treatment of the doped powders. In particular, a flash soaking into a tubular furnace kept at a fixed temperature in the range 1050–1150 °C was employed, for inducing the crystallization of yttrium-aluminates on the alumina particles surface, but avoiding a relevant crystallites growth. After that, aqueous suspensions of the calcined powders were dispersed by ball-milling and cast into porous moulds or simply dried in a oven. Slip cast green bodies were densified by pressure-less sintering, while powdered samples were consolidated by hot pressing or spark plasma sintering. The low- and high-temperature mechanical performances of the sintered materials were investigated and related to monolithic aluminas behaviour as well as to the composites microstructures. It is shown that the hot-pressed and spark plasma sintered composites present a significantly lower creep rate as compared to reference, monolithic alumina samples.

Keywords: B. Composites; B. Microstructure-final; C. Creep; D. Al_2O_3; YAG

1. Introduction

Alumina is largely used in industrial applications thanks to its excellent chemical stability and good mechanical properties, such as relevant fracture strength and very high hardness [1]. In addition, the high-temperature creep behaviour of polycrystalline alumina can be effectively increased by doping with small amounts (in the range 100–1000 ppm) of cations [2]. Among the various dopants tested [2], yttrium was largely used [3]: due to its limited solubility into the alumina lattice [4], it tends to segregate at the grain boundaries, thus reducing the inter-granular diffusion. Moreover, at high temperature, alumina grain growth can occur, and thus the yttrium content at grain boundaries can increase up to saturation. As a consequence, yttrium aluminum garnet (YAG) can precipitate and further affect both room and high-temperature properties of alumina [4]. For this reason, several recent papers focused on the Al_2O_3–YAG system [5–8], whose constituent phases exhibit mutual insolubility, high chemical stability and similar thermal expansion coefficients [9].

Li and Gao [5] prepared an Al_2O_3–5 vol.% YAG nano-composite by co-precipitation route and hot-pressing, yielding a microstructure made of an alumina matrix of about 0.6–1 μm in which both inter- and intra-granular YAG grains were dispersed. The authors determined an increase in Vickers hardness, fracture strength and fracture toughness of about 13, 56 and 25%, respectively, as compared to the reference monolithic alumina.

The high-temperature fracture toughness as well as the tensile creep behaviour of an Al_2O_3–50 vol.% YAG duplex, micron-sized microstructure was investigated by French et al. [9,10]. Their results showed that above 800 °C the composite provides higher toughness than the single-phase constituents, due to the toughening contribution of the interphase boundaries. In

* Corresponding author. Tel.: +39 011 5644678; fax: +39 011 5644699.
E-mail address: paola.palmero@polito.it (P. Palmero).
[1] Now at CEA Saclay DSM/IRAMIS/SPAM/LFP, Bat.522 91191 Gif sur Yvette, France.

0272-8842/$36.00
doi:10.1016/j.ceramint.2011.07.024

addition, in the temperature range 1100–1350 °C, the creep rate of the composite was lower than the respective monolithic phases. The mechanism proposed was a diffusional creep controlled by an interface reaction. Duong and Wolfestine [11] investigated the creep behaviour of Al_2O_3–50 vol.% YAG and Al_2O_3–75 vol.% YAG fine-grained composites: the authors indicated that the creep rate was controlled by YAG, which was the more creep-resistant phase, and suggested a diffusional Nabarro–Herring mechanism. The same behaviour was found by Torrecillas et al. [8,12] who produced an Al_2O_3–YAG nanocomposite by a colloidal processing route and pressure-less sintering, determining a creep rate one order of magnitude lower than that of pure alumina.

In this work, Al_2O_3–5 vol.% YAG composite powders were prepared by surface doping of α-alumina powders with a yttrium chloride aqueous solution. Two commercial alumina powders, differing on the mean particles size (about 150 and 600 nm, respectively) were compared as matrix materials. YAG phase was yielded by an in situ reaction promoted by the subsequent thermal treatment of the doped powders. With respect to the previous Literature, this work is aimed to investigate the effect of different densification routes on the mechanical behaviour of alumina–5 vol.% YAG at room and particularly at high-temperature, also exploring the role of the starting matrix powder on the composites microstructural features.

2. Materials

The elaboration of Al_2O_3–5 vol.% YAG composites was carried out by following a procedure already described in literature [13]. Briefly, surface modification of commercial alumina powders by a yttrium inorganic salt was performed. Upon heating, a solid state reaction between a part of alumina and the yttrium-rich precursor yielded the composite powders [14].

Two commercial α-alumina powders were employed. The former, TM-DAR TAIMICRON (referred to as T), is supplied by TAIMEI Chemical Co. (Japan) and is characterized by a mean grain size of about 150 nm and a specific surface area of 14.5 m^2/g [15]. The latter, CR1 (referred to as C), is supplied by Baikowski (France) and is characterized by an average particle size of 0.6 μm and a specific surface area of 3 m^2/g [16]. Both alumina powders are characterized by high purity (>99.99%), as declared by the suppliers [15,16]. The main impurities of T powder are Si (10 ppm), Na (8 ppm) and Fe (8 ppm); the ones of the C powder are Si (40 ppm), K (22 ppm), Na (13 ppm), Fe (7 ppm), Ca (3 ppm) and Mg, Ti, Cr, Mn, Ni, Cu, Zn (less than 1 ppm, each). Dispersed slurries of the alumina powders were mixed with suitable amounts of an aqueous solution of $YCl_3{\cdot}6H_2O$ (Sigma–Aldrich, 99.99% purity). After spray-drying [13], the powders were pre-treated at 600 °C for 1 h, in order to allow by-products (mainly chlorides) decomposition, as detailed in a previous paper [14]. A subsequent thermal treatment was carried out by instantaneously plunging the powders into a tubular furnace kept at a fixed temperature in the range 1050–1150 °C for a short time (3 min), in order to minimize powder aggregation and crystallites growth [17]. The composite powders are hereafter referred to as YT and YC.

Aqueous suspensions of YT and YC, at a solid loading of 50 wt.%, were dispersed by ball-milling for 24 h, at their natural pH (around 5.5) to avoid yttrium dissolution which can occur into acid media [18].Then, they were cast into porous moulds or simply dried in a oven. Slip cast green bodies were densified by pressure-less sintering (PS), while powdered samples were consolidated in dense pieces by hot pressing (HP) or by spark plasma sintering (SPS).

In particular, PS was performed up to 1500 °C for 3 h (heating rate of 10 °C/min up to 1100 °C and then at 2 °C/min up to 1500 °C, on the ground of preliminary dilatometric studies [19]).

HP samples were sintered in pellets, 20 or 40 mm in diameter, by heating up to 1450 °C for 1 h (heating rate of 10 °C/min up to 1100 °C and 2 °C/min up to 1450 °C) under a pressure of 75 MPa.

Finally, SPS samples were prepared by heating up to 1350 (YT sample) or 1450 °C (YC), under a stress of 75 MPa. The heating rate and the soaking time were 150 °C/min and 3 min, respectively. This process was followed by a second dwell time at 1060 °C (cooling rate of about 600 °C/min) for 5 min.

Pure alumina samples were also prepared as reference materials: dispersed slurries of T and C powders were slip cast and pressure-less sintered (referred to as T/PS and C/PS, respectively) under the previously given conditions.

A scheme of the samples preparation is presented in Fig. 1, including samples designations and some experimental details.

3. Characterization techniques

3.1. Physical and microstructural characterizations

The final density of the composites was determined by the Archimedes' method and referred to the theoretical density

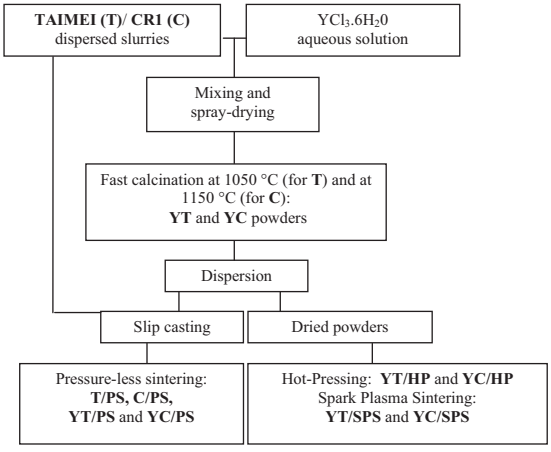

Fig. 1. Flow-chart of the samples elaboration and their designations.

(TD) calculated by the rule of the mixture, using 3.99 g/cm^3 for α-alumina [20] and 4.55 g/cm^3 for YAG [21].

The microstructural characterization of the sintered bodies were performed by Field Emission Scanning Electron Microscopy (FESEM Hitachi S4000), carried out on polished and thermally etched surfaces. The grains sizes were measured by using an image analysis software (Scandium soft imaging system) and the mean value was calculated by using the linear intercept method in the horizontal and vertical directions on at least a hundred grains.

3.2. R.T. mechanical characterization

Vickers hardness (HV) measurements were carried out on sintered samples by using Tester FV-7. Indentations were made on polished surfaces under a load of 98.1 N (10 kg) held for 10 s. Average hardness values and standard deviations were calculated from the results of five measurements.

Young's modulus (E) was determined by the impulse excitation technique. The tests were performed on bar-shaped samples at room temperature according to the ASTM standards C1259-01.

Fracture toughness (K_{IC}) was estimated using the Anstis' formula [22]:

$$K_{IC} = A \cdot \left(\frac{E}{H}\right)^{1/2} \cdot \left(\frac{P}{c}\right)^{2/3} \quad (1)$$

where A is a geometrical constant, equal to 0.016; E is the Young's modulus experimentally determined as previously described; H is the Vickers hardness; P is the applied load; c is the crack length measured from the centre of indentation to the end of the crack.

3.3. H.T. mechanical characterization

Creep tests on pure alumina and composite samples were performed in a 4-point-bending fixture at a temperature of 1200 °C (heating rate of the furnace of 300 °C/h) under an applied stress of 100 MPa.

Tests were performed on bars of about 3 mm (sample height) × 4 mm (width) × 32 mm (length); the tensile surface of all the specimens was polished with diamond paste down to 3 μm and the edges were chamfered (about 45°) in order to avoid the influence of microcracks during creep. The creep tests were carried out until the rupture of the samples.

Inner and outer spans of the 4-point-bending fixture were 15 and 30 mm, respectively. The flexural stress on the tensile face of the specimen was calculated employing the following expression:

$$\sigma = \frac{3P(L - L')}{2bw^2} \quad (2)$$

where P is the applied load, L is the outer span, L' is the inner span, b is the sample width and w is the sample height.

To determine the creep strain ε, the method by Hollenberg et al. [23] was used, based on the assumption that ε can be calculated from the deflection y at the centre of the specimen if there is no major cracking and if y is small compared with the inner span:

$$\varepsilon = K(n) \cdot y \quad \text{where} \quad K(n) = \frac{2w(n+2)}{(L - L')[L - L'(n+1)]} \quad (3)$$

It was shown [23] that for L/L' values close to 2, $K(n)$ is almost insensitive to n. So, expression (3) can be used and ε calculated with an approximate value for n. In case of a too high divergence between the determined and initial supposed n values, ε must be recalculated.

The steady-state creep rate $\dot{\varepsilon}$ is defined by the following equation:

$$\dot{\varepsilon} = A\frac{\sigma^n}{d^p}\exp\left(-\frac{Q}{RT}\right) \quad (4)$$

where A is a material constant; σ is the applied stress; n is the stress exponent; d is the grain size; p is the grain size exponent; Q is the activation energy for creep; R is the gas constant and T is the absolute temperature.

Finally, to compare the creep behaviour of the investigated materials, creep rates were normalized by using the following equation [8]:

$$\dot{\varepsilon}_n = \left(\frac{1}{d_A/d_B}\right)^P \cdot \dot{\varepsilon}_B \quad (5)$$

where $\dot{\varepsilon}_n$ is the normalized creep rate; $\dot{\varepsilon}_B$ is the measured creep rate; d_A is the mean alumina grain size in T/PS and C/PS materials; d_B is the mean grain size of the composite and p the grain size exponent. Creep was assumed to be controlled by lattice diffusion [12], so that creep rates were normalized taking p equal to 2 [24].

4. Results and discussion

4.1. Physical and microstructural characterizations

The final densities of all specimens are collected in Table 1.

For what concerns the PS samples, data show that in the employed pressure-less conditions, ultra-fine starting alumina particles (such as T) are required to yield fully dense alumina

Table 1
Final density and average Al_2O_3 and YAG grain sizes of the sintered samples.

Sample	Final density (%TD)	Average grain size (μm)	
		Al_2O_3	YAG
T/PS	99.4	1.00 ± 0.21	–
YT/PS	99.7	0.64 ± 0.24	0.24 ± 0.07
YT/HP	98.5	1.07 ± 0.50	0.58 ± 0.18
YT/SPS	99.4	1.29 ± 0.83	0.30 ± 0.13
C/PS	97.4	2.61 ± 1.21	–
YC/PS	94.4	0.92 ± 0.28	0.43 ± 0.14
YC/HP	98.9	1.10 ± 0.38	0.45 ± 0.15
YC/SPS	99.7	1.31 ± 0.53	0.50 ± 0.15

bodies [25]. Similarly, the T-derived composites reached full densification, whereas a poor final value was obtained by YC/PS. Differences in starting alumina features seem to be arisen by the non-conventional sintering routes: in fact, both YT and YC samples showed very high final densities, especially after SPS.

From FESEM observations, the pure alumina samples (Fig. 2) present quite relevant differences in microstructural features. The heterogeneous microstructure of T/PS (Fig. 2(a)) is characterized by some abnormal elongated grains of more than 10 μm, surrounded by a quite homogeneous, micron-sized matrix. Such coarsened grains can be probably due to the prolonged soaking time (3 h) at high temperature (1500 °C) of a material able to fully sinter at a lower temperature, as stated in recent literature [13,19]. On the other hand, C/PS (Fig. 2(b)) is mostly made of equiaxial grains with an average size of about 2.6 μm; some inter- and intra-granular pores can be also observed, according to the moderate final density of this material.

In Fig. 3, the micrographs of YT/PS (a), YT/HP (b) and YT/SPS (c) are collected.

The PS sample presents a highly homogeneous microstructure, made of alumina grains of about 0.65 μm in size and a well-distributed, ultra-fine second phase. YAG grains are mainly located at the grain boundaries or at triples joints, and exhibit a size in the range 200–300 nm. In addition, if Figs. 2(a) and 3(a) are compared, the effective *pinning* [26,27] exerted by YAG nanograins on the alumina grain boundaries can be assessed since abnormally grown alumina grains were never observed in YT/PS.

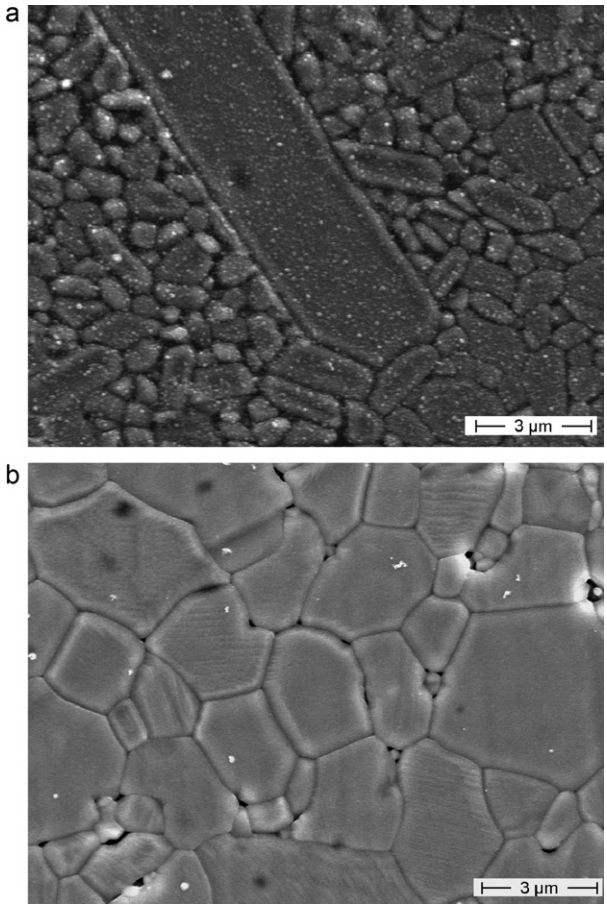

Fig. 2. FESEM micrographs of pure T/PS (a) and C/PS (b) samples.

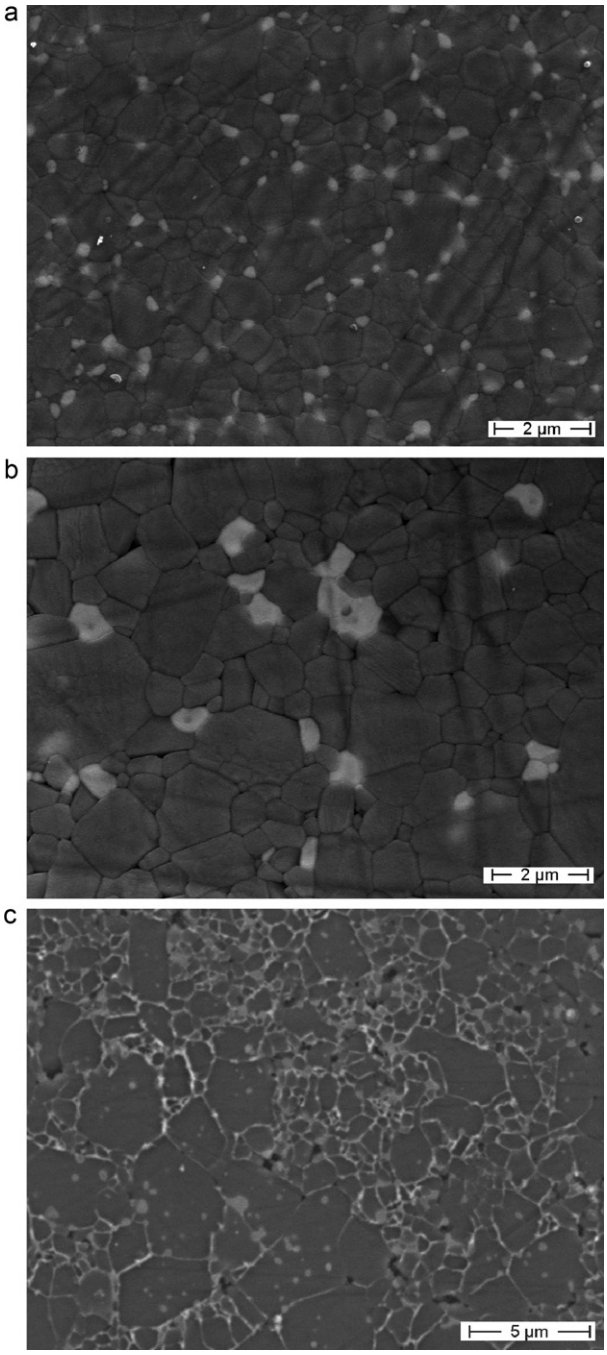

Fig. 3. FESEM micrographs of YT/PS (a), YT/HP (b) and YT/SPS (c).

On the contrary, YT/HP sample presents an overall coarsened microstructure: a significant growth of both alumina and YAG grains occurred during hot-pressing, leading to a microstructure made of second-phase particles of 500–800 nm in size dispersed into a micron-sized matrix. YAG grains were predominantly located at inter-granular positions, in spite of few second-phase particles entrapped within alumina grains.

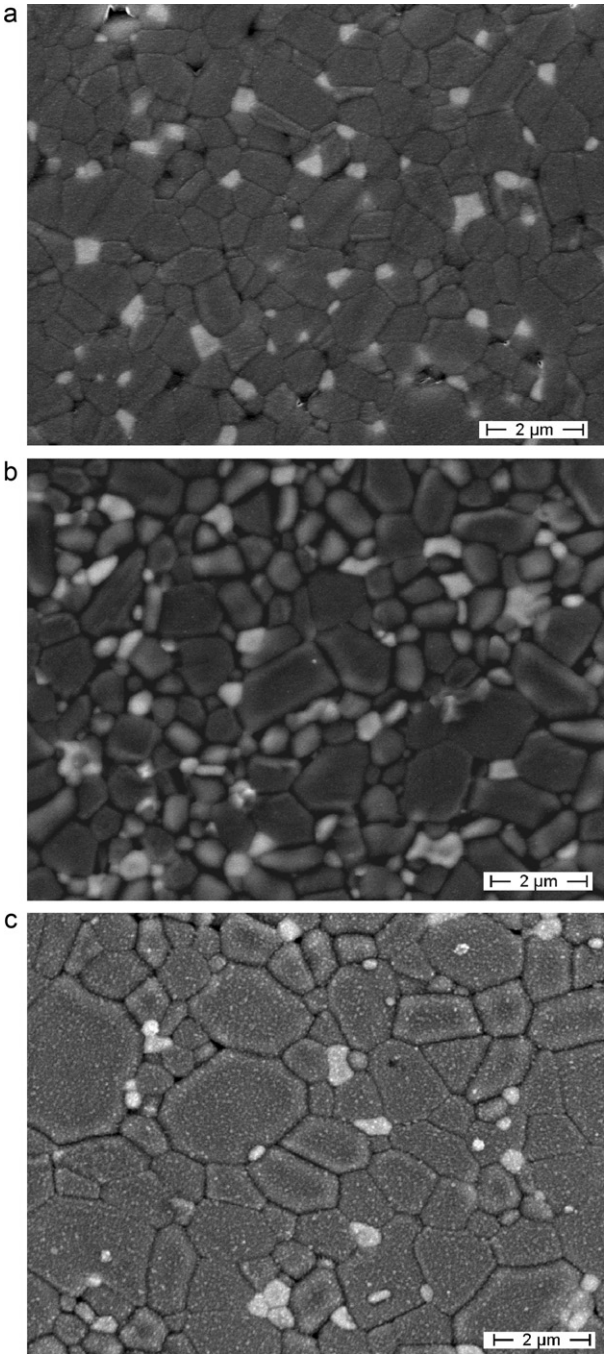

Fig. 4. FESEM micrographs of YC/PS (a), YC/HP (b) and YC/SPS (c).

For what concerns YT/SPS, a heterogeneous microstructure was produced. In fact, a bimodal grain size distribution was determined for the alumina phase, since several large grains (some microns in size) were embedded into a finer matrix. YAG particles (with a mean size of 300 nm) were prevalently located in intergranular position, in spite of few second-phase grains within the larger alumina grains.

In Fig. 4, the microstructures of YC/PS (a), YC/HP (b) and YC/SPS (c) are compared.

Once again, the PS material is characterized by homogeneously dispersed, fine YAG particles located into a micron-sized alumina matrix. YAG grain size ranges between 400 and 500 nm and particles are mainly located at the grain boundaries or at triple points. However, as expected on the ground of its poor final density, YC/PS presents a significant residual porosity, mainly made of inter-granular pores.

In contrast, almost fully dense microstructures were produced by HP and SPS. Both materials are characterized by micron-sized, almost equiaxial alumina grains, and by a homogeneous dispersion of YAG particles of about 450 nm in size. However, by comparing the three microstructures of Fig. 4, we can observe that the finer alumina matrix is present in the PS material, the larger in the SPS one. In contrast, YAG grain size was quite similar in the three composites.

For the sake of clarity, the average alumina and YAG grain sizes of all the sintered materials are collected in Table 1.

4.2. R.T. mechanical characterization

In Table 2, Vickers hardness and fracture toughness values for the fired specimens are collected.

All samples present high hardness values, ranging between about 18 and 20 GPa; as expected, the higher HV values were determined for the denser materials (see values in Table 1). Few hardness data are reported in literature for alumina–YAG ultra-fine-grained composites; however, as a comparison, a HV value of 16.15 GPa was found by Li and Gao [5] for a hot-pressed, fully dense alumina–25 vol.% YAG composite, made by a homogeneous distribution of fine (100–800 nm) YAG grains into the alumina matrix.

Considering the fracture toughness, the sintering route appears to play a major role. In fact, less-conventional processes led to tougher materials, especially for YC/SPS samples, whose K_{IC} is close to 7 MPa $m^{1/2}$. In order to explain this result, the fracture surfaces of the samples were systematically observed: both inter- and trans-granular fracture paths were present in all samples; however, the trans-granular fracture mode was more frequently observed in the HP and SPS materials, as compared to the PS ones. For sake of clarity, the fracture surface of YT/PS (a), YT/HP (b) and YT/SPS (c) are compared in Fig. 5: the clear evidence of trans-granular crack paths found in HP and SPS samples is highlighted by the arrows in Fig. 5(b) and (c). Moreover, the higher K_{IC} values of the HP and SPS samples can be also due to their overall coarser microstructure, if compared to PS materials (see data in Table 1). In fact, as reported by Swain [28], the fracture toughness of alumina and alumina-based composites increases linearly as a function of $d^{1/2}$.

As a comparison, fracture toughness in the range 3–5.8 MPa $m^{1/2}$ were determined for YAG-reinforced alumina

Table 2
Vickers hardness (HV) and fracture toughness (K_{IC}) of the sintered samples.

Sample	HV (GPa)	K_{IC} (MPa $m^{1/2}$)
YT/PS	18.8 ± 1.13	4.4
YT/HP	18.0 ± 0.88	6.2
YT/SPS	19.9 ± 0.5	5.8
YC/PS	18.7 ± 0.49	4.7
YC/HP	19.7 ± 1.10	6.4
YC/SPS	19.0 ± 0.64	7.3

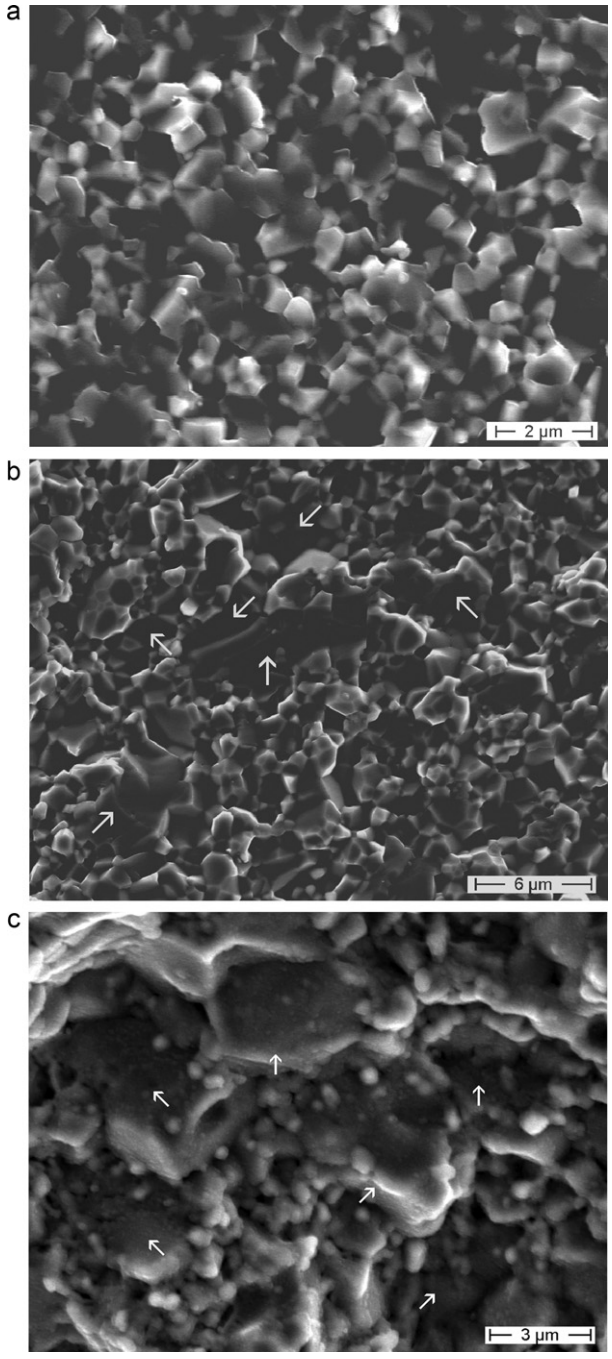

Fig. 5. FESEM micrographs of the fracture surfaces of YT/PS (a), YT/HP (b) and YT/SPS (c).

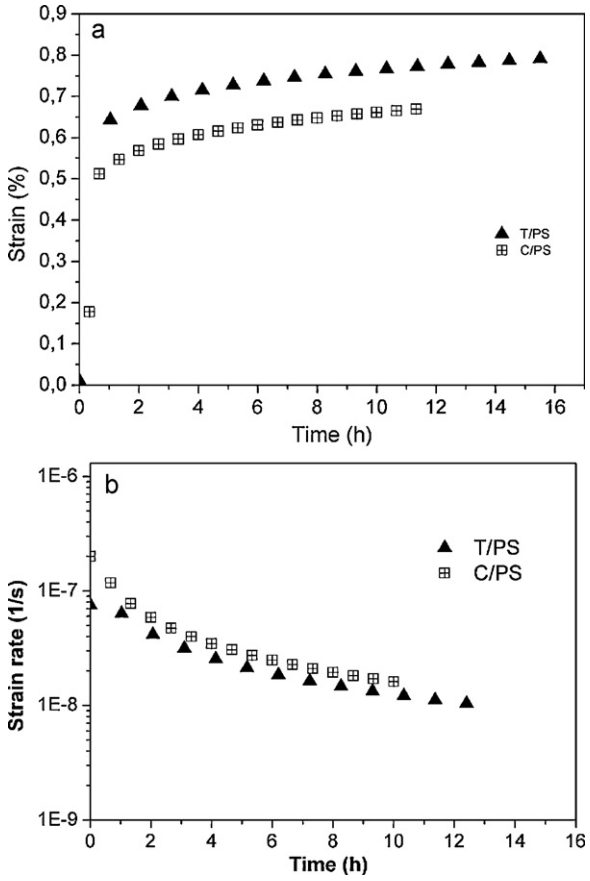

Fig. 6. Strain (a) and strain rate (b) as a function of time for T/PS and C/PS at 1200 °C and 100 MPa.

micro/nanocomposites, having YAG phase amount ranging between 5 and 50 vol.% [5–9].

Finally, the Young's moduli of YT/PS and YC/PS were determined, and the values of 419.2 and 415.5 GPa, respectively, were in good agreement with the modulus of 409.2 GPa, calculated by the rule of the mixture.

4.3. H.T. mechanical characterization

The creep curves of T/PS and C/PS aluminas are shown in Fig. 6(a). Two stages, a transient and a steady-state step, are present. The deformation (ε) was lower than 1% in both samples, being 0.79% for T/PS and 0.67% for C/PS, respectively.

The creep rate (Fig. 6(b)) was determined by the slope of the creep curve: in both samples, it slightly decreases without reaching a constant value, corresponding to the stationary creep stage. The creep rate values after about 10 and 12 h for C/PS and T/PS, respectively, are collected in Table 3. The two alumina samples present similar deformation rates, in spite of their quite different microstructures. In fact, a higher deformation rate was expected for T/PS alumina, being its average grain size significantly lower than C/PS one. However, the presence of abnormally grown as well as tabular grains in a fine matrix in T/PS seems to be very effective in limiting the

Table 3
Raw and normalized strain rates of the sintered samples.

Sample	Raw creep rate (s^{-1})	Normalized creep rate (s^{-1})
T	1.04×10^{-8}	1.04×10^{-8}
YT/PS	1.89×10^{-8}	7.74×10^{-9}
YT/HP	5.47×10^{-9}	6.26×10^{-9}
YT/SPS	1.91×10^{-9}	3.18×10^{-9}
C	1.61×10^{-8}	1.61×10^{-8}
YC/PS	5.26×10^{-8}	6.54×10^{-9}
YC/HP	5.41×10^{-9}	9.61×10^{-10}
YC/SPS	2.26×10^{-9}	5.69×10^{-10}

deformation rate, as compared to the almost equiaxed microstructure of C/PS material. In addition, this latter sample presents some residual pores which can improve the creep rate, as shown by Langdon [29].

The same approach was then applied to the composites. In Fig. 7, the evolution of the creep as a function of time is shown for the sintered YT (a) and YC (b) composites. The deformation of all the YT samples was significantly lower than in pure T/PS, being 0.23% for YT/PS, 0.26% for YT/HP and 0.11% for YT/SPS, respectively. In the last case, the deformation is seven times lower than in T/PS.

Creep rates (raw and normalized data) after about 30 h test are collected in Table 3 and also drawn in Fig. 8(a).

If raw data are concerned, the higher strain rate of YT/PS can be readily observed. Its microstructure can easily justify such experimental evidence: in fact, as shown in Table 1, YT/PS presents the finer alumina matrix, thanks to the highly homogeneous distribution of ultra-fine YAG particles inside it. This feature promotes sliding phenomena among the alumina grain boundaries, so that high-temperature deformation can rapidly occur.

In contrast, both YT/HP and YT/SPS samples present a better creep behaviour, being their creep rates about 3.5 and 10 times, respectively, lower than that of YT/PS. The coarsened microstructures of the non-conventionally sintered samples make these materials more suitable for high-temperature

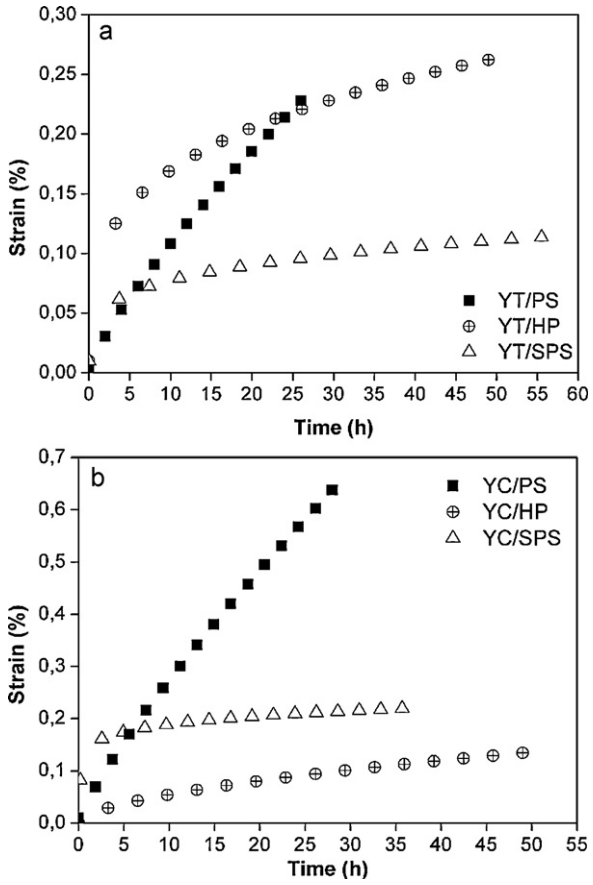

Fig. 7. Strain as a function of time for YT (a) and YC (b) samples at 1200 °C and 100 MPa.

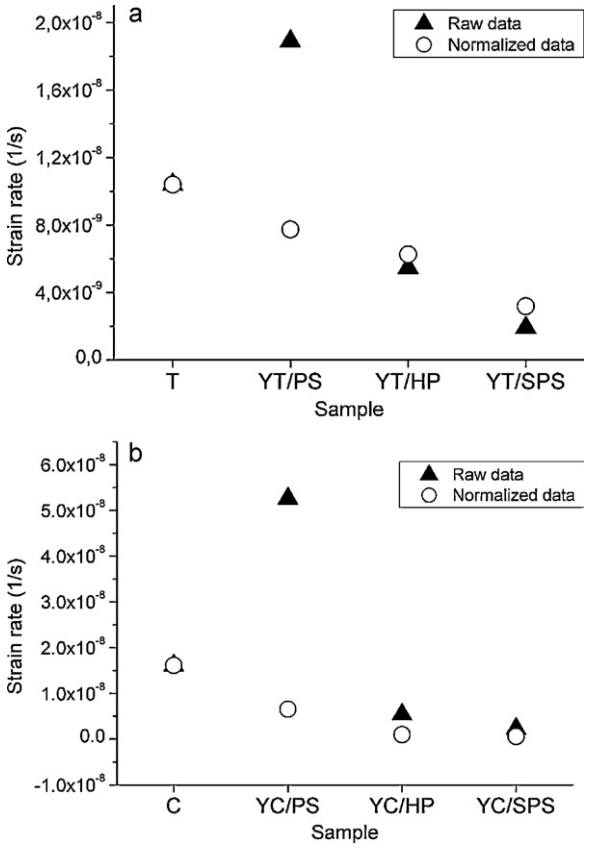

Fig. 8. Raw and normalized strain rates of T-derived (a) and C-derived (b) materials.

applications. In addition, the heterogeneous microstructure of YT/SPS, in which alumina grains present a bimodal size distribution, provide a further reduction of the deformation rate.

Normalized data allowed to better assess the role of YAG in decreasing the creep rate of alumina, even in the case of the slight effect associated to YT/PS. The lower creep rate of the composites can be, in fact, reasonably imputed to the presence of YAG particles at the alumina grain boundaries. Several papers in the past discussed the role of yttrium and of yttrium-aluminates on the creep behaviour of alumina [4,11,30]. Segregation of yttrium at alumina grain boundaries has been imputed to the larger Y ionic radius ($r = 0.093$ nm) as compared to the Al one ($r = 0.041$ nm) and to the very low yttrium solubility into α-Al_2O_3 lattice (less than 10 ppm) [4]. Such large ions are able to block the diffusion along the alumina grain boundaries, with a consequent reduction in grain boundary diffusivity and decrease in creep rate [3,8]. A more recent paper [31] has elucidated the atomic-scale structure of alumina grain boundaries and its relationship to the suppression of creep upon doping with yttrium. In Y-doped alumina, Y^{3+} does not alter the basic grain boundary structure since it simply replaces Al^{3+} at specific sub-lattice sites. In addition, static lattice calculations proved the role of yttrium in drastically changing the chemical bonds state of the surrounding atoms (precisely from a mainly ionic-type bonding in pure alumina to covalent-type in doped samples), with the effect of improving the grain boundary strength against creep.

In our work, however, the yttrium content is significantly higher than the alumina solubility limit, so that YAG second particles are formed. In this case, the sliding of alumina grains is blocked by the presence of YAG (nano)particles and it is allowed only if YAG grains are deformed. However, the high activation energy required to deform YAG [10,32] can explain the better behaviour of the composites as compared to the neat matrix.

The strain versus time plot of YC samples is presented in Fig. 7(b). All the samples show lower deformations as compared to the neat matrix: in fact values of 0.64, 0.13 and 0.22% were respectively found for YC/PS, YC/HP and YC/SPS.

The raw and normalized creep rates after about 30 h test are collected in Table 3 and drawn in Fig. 8(b).

If raw data are considered, the final density (see Table 1) seems to play the major role on the creep behaviour. In fact, the fully dense YC/SPS and YC/HP show lower deformation rates as compared to pure C/PS, whereas a significant increase was determined for YC/PS, characterized by a significant residual porosity. When normalized rates are concerned, YC/PS, YC/HP and YC/SPS show a reduction of about 2.5, 17 and 28 times, respectively, in comparison with pure C/PS. The creep rate determined for YC/SPS is in a very good agreement with the value given by Schehl et al. [12], who found a non-normalized creep rate of 2.0×10^{-9} s^{-1} (creep test at 1200 °C, under an applied stress of 100 MPa).

Finally, Fig. 9 compares the creep rates of YT and YC samples (raw data are used), to discuss the role of the starting alumina on the high-temperature mechanical behaviour of the composites, which appears to be crucial especially when PS is applied.

The different features which characterize the starting T and C powders play a double role on the PS samples. By one side, they affect the densification behaviour, leading to fully dense composites if the nanometric T powder is used (as in the case of YT/PS) and to poorly densified materials if derived by the sub-micrometric C powder (as for YC/PS). By the other side, they induce a different microstructural development, since YT/PS presents a microstructure close to a nano/nano-composite [33], whereas an almost micro/nano-composite [33] is yielded by YC/PS. The better creep behaviour of YT/PS strengthen, in this particular case, the key role of the final density [29] over the microstructural features in limiting the deformation rate.

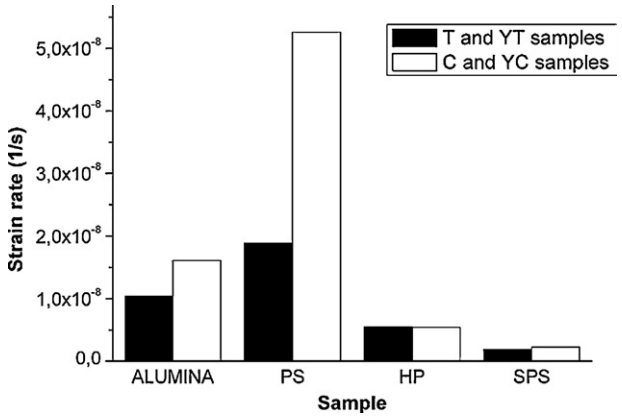

Fig. 9. Raw strain rates of YT and YC samples.

The strain rates of the HP samples were almost the same, independently from the starting alumina powders. In fact, hot-pressing induces a significant grain growth, thus to annihilate the differences in starting alumina features.

Also YT/SPS and YC/SPS samples behave similarly, in spite of their quite different microstructures. The bimodal grain size distribution which characterize the alumina matrix in YT/SPS seems to be very effective in reducing the creep rate, if compared to the more homogeneous, equiaxial microstructure of YC/SPS.

5. Conclusions

The role of the starting α-alumina powders features and of the densification routes (PS, HP, SPS) on final density, microstructural development, low- and high-temperature mechanical properties of six different Al_2O_3–5 vol.% YAG composites were investigated, from which the following conclusions can be drawn out:

(i) The starting α-alumina features affect both final densities and microstructures when PS is applied: a fully dense, ultra-fine composite is yielded when T powder is used, whereas a significant porosity and an almost micro/nano-structure were produced in the C-derived sample. Such differences were mostly arisen by non-conventional sintering routes, since high final densities and overall coarsened microstructures were obtained by both HP and SPS, independently from the starting alumina powder;

(ii) All samples present high Vickers hardness (18–20 GPa), the higher values being associated to the denser materials. The sintering process plays, indeed, the major role on the fracture toughness: non-conventional routes lead to the tougher materials, mainly due to a change of fracture path from rather inter-granular in PS sample to a trans-granular mode in the HP and SPS materials;

(iii) By taking the creep behaviour of T and C neat matrix as a reference, both final density and microstructural features were found to affect the creep rate of the composites. The T-derived PS sample presents a relevant creep rate due to its ultra-fine microstructure which can promote sliding phenomena among the alumina grain boundaries. However, a considerably higher value was determined for the C-derived material, whose coarsened microstructure was however affected by a significant residual porosity. Non-conventionally sintered materials present better creep behaviours, independently from the starting alumina powders, due to their microstructures made by a micron-sized matrix, in which a quite good distribution of YAG grains of about 0.5–0.6 μm is produced. Finally, comparing HP and SPS samples, a slightly lower creep rate was determined for the latter ones, exhibiting the higher final densities.

References

[1] Y. Yoshizawa, K. Hirao, S. Kanzaki, Fabrication of low cost fine-grained alumina powders by seeding for high performance sintered bodies, J. Eur. Ceram. Soc. 24 (2004) 325–330.

[2] H. Yoshida, Y. Ikuhara, T. Sakuma, High temperature plastic deformation related to grain boundary chemistry in cation-doped alumina, Mater. Sci. Eng. A 387–389 (2004) 723–727.
[3] J. Cho, M.P. Harmer, H.M. Chan, J.M. Rickman, A.M. Thompson, Effect of yttrium and lanthanum on tensile creep behaviour of aluminum oxide, J. Am. Ceram. Soc. 80 (1997) 1013–1017.
[4] S. Lartigue-Korineka, C. Carry, L. Priester, Multiscale aspects of the influence of yttrium on microstructure, sintering and creep of alumina, J. Eur. Ceram. Soc. 22 (2002) 1525–1541.
[5] W.Q. Li, L. Gao, Processing, microstructure and mechanical properties of 25 vol% YAG–Al_2O_3 nanocomposites, Nanostruct. Mater. 11 (1999) 1073–1080.
[6] H. Wang, L. Gao, Preparation and microstructure of polycrystalline Al_2O_3–YAG composites, Ceram. Int. 27 (2001) 721–723.
[7] H. Wang, L. Gao, Z. Shen, M. Nygren, Mechanical properties of Al_2O_3–5 vol.% YAG composites, J. Eur. Ceram. Soc. 21 (2001) 779–783.
[8] M. Schehl, L.A. Diaz, R. Torrecillas, Alumina nanocomposites from powder–alkoxide mixtures, Acta Mater. 50 (2002) 1125–1139.
[9] J.D. French, H.M. Chan, M.P. Harmer, G.A. Miller, High-temperature fracture toughness of duplex microstructures, J. Am. Ceram. Soc. 79 (1996) 58–64.
[10] J.D. French, J. Zao, M.P. Harmer, H.M. Chan, G.A. Miller, Creep of duplex microstructures, J. Am. Ceram. Soc. 77 (1994) 2857–2865.
[11] H. Duong, J. Wolfestine, Creep behaviour of fine-grained two-phase Al_2O_3–$Y_3Al_5O_{12}$ materials, Mater. Sci. Eng. A 172 (1993) 173–179.
[12] R. Torrecillas, M. Schehl, L.A. Diaz, J.L. Menendez, J.S. Moya, Creep behaviour of alumina/YAG nanocomposites obtained by colloidal processing route, J. Eur. Ceram. Soc. 27 (2007) 143–150.
[13] P. Palmero, V. Naglieri, J. Chevalier, G. Fantozzi, L. Montanaro, Alumina-based nanocomposites obtained by doping with inorganic salt solutions. Application to immiscible and reactive systems, J. Eur. Ceram. Soc. 29 (2009) 59–66.
[14] P. Palmero, C. Esnouf, Phase and microstructural evolution of yttrium-doped nanocrystalline alumina. A contribution of advanced microscopy techniques, J. Eur. Ceram. Soc. 31 (2011) 507–516.
[15] http://www.taimei-chem.co.jp.
[16] http://www.baikowski.com.
[17] P. Palmero, V. Naglieri, G. Spina, M. Lombardi, Microstructural design and elaboration of multiphase ultra-fine ceramics, Ceram. Int. 37 (2011) 139–144.
[18] J.C. Farinas, R. Moreno, J. Requena, J.S. Moya, Acid-basic stability of Y-TZP ceramics, Mater. Sci. Eng. A 109 (1989) 97–99.
[19] P. Palmero, V. Naglieri, L. Montanaro, Preparation and characterization of alumina-doped powders for the design of multi-phasic nano-microcomposites, J. Therm. Anal. Calorim. 97 (2009) 231–237.
[20] JCPDS file n. 46-1212.
[21] JCPDS file n. 33-0040.
[22] G. Anstis, P. Chantikul, B. Lawn, A critical evaluation of indentation techniques for measuring fracture toughness, J. Am. Ceram. Soc. 64 (1981) 533–538.
[23] G.W. Hollenberg, G.R. Terwellinger, R.S. Gordon, Calculation of stresses and strains in four-point bending creep tests, J. Am. Ceram. Soc. 54 (1971) 196–199.
[24] C. Herring, Diffusional viscosity of a polycrystalline solid, J. Appl. Phys. 21 (1950) 437–445.
[25] R.S. Averback, H.J. Hofler, R. Tao, Processing of nano-grained materials, Mater. Sci. Eng. A 166 (1993) 169–177.
[26] L. Stearns, M.P. Harmer, Particle-inhibited grain growth in Al_2O_3–SiC. I. Experimental results, J. Am. Ceram. Soc. 79 (1996) 3013–3019.
[27] C.-J. Wang, C.-Y. Huang, Y.-C. Wu, Two-step sintering of fine alumina–zirconia ceramics, Ceram. Int. 35 (2009) 1467–1472.
[28] M.V. Swain, Structure and properties of ceramics, in: R.W. Cahn, P. Haasen, E.J. Kramer (Eds.), Materials Science and Technology, vol. 11, VCH, Weinheim, 1994, pp. 452–454.
[29] T.G. Langdon, Dependence of creep rate on porosity, J. Am. Ceram. Soc. 45 (1962) 630–631.
[30] H. Yoshida, Y. Ikuhara, T. Sakuma, High-temperature creep resistance in rare-earth-doped fine-grained Al_2O_3, J. Mater. Res. 13 (1998) 2597–2601.
[31] J.P. Buban, K. Matsunaga, J. Chen, N. Shibata, W.Y. Ching, T. Yamamoto, Y. Ikuhara, Grain boundary strengthening in alumina by rare earth impurities, Science 311 (2006) 212–215.
[32] T.A. Parthasarathy, T.I. Mah, K. Keller, Creep mechanism of polycrystalline yttrium–aluminum-garnet, J. Am. Ceram. Soc. 75 (1992) 1756–1759.
[33] K. Niihara, New design concept of structural ceramics–ceramic nanocomposites, Centennial Memorial Issue of Ceram. Soc. Jpn. 99 (1999) 974–982.